Beyond Explored Functionals: A Computational Journey of Two-Photon Absorption

Ismael A. Elayan,[†] Laura Rib,[†] Rodrigo A. Mendes,[†,‡] and Alex Brown[*,†]

†*Department of Chemistry, University of Alberta, Edmonton, Alberta, Canada, T6G 2G2*

‡*Departamento de Química, Universidade Federal de Mato Grosso, Cuiabá, Mato Grosso, 78060-900 Brazil*

E-mail: alex.brown@ualberta.ca

Abstract

We present a thorough investigation into the efficacy of 19 DFT functionals, relative to RI-CC2 results, for computing two-photon absorption (2PA) cross-sections (σ^{2PA}) and key dipole moments (μ_{00}, μ_{11}, $\Delta\mu$, μ_{01}) for a series of coumarin dyes in the gas-phase. The functionals include different categories, including local density approximation (LDA), generalized gradient approximation (GGA), hybrid-GGA (H-GGA), range-separated hybrid-GGA (RSH-GGA), meta-GGA (M-GGA), and hybrid M-GGA (HM-GGA), with 14 of them being subjected to analysis for the first time with respect to predicting σ^{2PA} values. Analysis reveals that functionals integrating both short-range (SR) and long-range (LR) corrections, particularly those within the RSH-GGA and HM-GGA classes, outperform others. Furthermore, the range-separation approach was found more impactful compared to the varying percentages of Hartree-Fock exchange (HF E_x) within different functionals. The functionals traditionally recommended for 2PA do not appear among the top 9 in our study, which is particularly interesting as these top-performing functionals have not been previously investigated in this context. This list is dominated by M11, QTP variants, ωB97X, ωB97X-V, and M06-2X, surpassing the performance of other functionals, including the commonly used CAM-B3LYP.

1 Introduction

Two-photon absorption (2PA) is a third-order optical process that involves the simultaneous absorption of a pair of photons, where both photons could be of identical frequencies (degenerate, $\omega_1 = \omega_2$) or different frequencies (non-degenerate, $\omega_1 \neq \omega_2$). The total energy ($\omega_1 + \omega_2$) is equal to the excited state energy. In 1931, Maria Göppert-Mayer first theorized 2PA,[1] however, 2PA optical phenomena require intense light irradiation. Therefore, the first experimental evidence was reported 30 years later,[2] with the invention of lasers, through the observation of luminescence of a Eu-doped crystal in CaF_2:Eu. The measured 2PA is quantified by its probability, which is given as a cross-section (σ^{2PA}, provided in GM units, where 1 GM = 10^{-50} cm^4 s photon^{-1} molecule^{-1}).

The (degenerate) 2PA process is proportional to the square of the intensity of the incident light beam. On the other hand, the non-degenerate 2PA process is proportional to the product of the intensities of two separate light beams, which influences the values of σ^{2PA},[3,4] along with resonance enhancement.[5,6] Furthermore, 2PA utilizes longer excitation wavelengths than conventional one-photon absorption (1PA). These characteristics of 2PA result in increased penetration depth, improved spatial resolution, and minimized photobleaching to the sample, making it a desirable optical technique.[7] Consequently, 2PA has been used in microscopy of biological imaging,[8,9] photodynamic therapy,[10,11] 3D microfabrication,[12,13] and optical data storage,[14,15] to name a few. As these applications continue to evolve, so does the quest for efficient 2PA dyes with large cross-sections.[16]

The design of dyes with large cross-sections requires an understanding of the photophysical properties, long-range charge transfer, structural substituent effects, and solvatochromism of the systems of interest.[17–19] However, the determination of such properties of fluorescent dyes is a complex process since several factors affect them, such as the used measurement method, absorption and emission wavelengths, chemical structures, quantum yield, and sol-

vent.[20–23] In this area, computational chemistry has emerged as a valuable asset,[24–28] where it serves as a useful tool to elucidate experimental findings as well as examine various properties, such as excited state energies (ΔE),[29–31] oscillator strengths (f),[32,33] dipole moments (μ),[34,35] and their influence on the values of σ^{2PA}.[36,37]

The use of response theory and implemented correlated wavefunction theory (WFT) second-order approximate coupled-cluster, CC2,[38] in conjunction with the resolution-of-identity approximation, RI-CC2,[39] as well as time-dependent density-functional theory (TD-DFT)[40] makes it possible to compute the photophysical properties of interest for 2PA. Available TD-DFT approaches can depend on the quantum chemistry software package selected and functionals implemented therein, where a coupled-cluster method often serves as a reference.[41] However, these simulations can be challenging, given the influence of multiple factors, such as vibronic effects, the surrounding environment, and the size of the system; thus, restricting the ability to agree, or even qualitatively compare, with experimental results.[30,37] Furthermore, the challenge persists in determining a suitable functional, one that balances both quantitative precision and qualitative insights. While various TD-DFT functionals are available, the range-separated hybrid (RSH), CAM-B3LYP, remains as the go-to source for excited states in many 2PA calculations.[42] For 1PA excited state properties, the values of ΔE and f have been investigated for different systems using a wide-range of methods climbing Jacob's ladder of functionals.[29,32,33,43–49] On the other hand, for 2PA cross-sections, which is the interest of this work, existing benchmarks have only shed light on a few functionals, leaving a vast number to explore.[35,36,41,42,50–52] This missing benchmarking raises the question about the efficacy of these unexplored functionals, when predicting σ^{2PA} values, which are influenced by the transition and permanent dipole moments (μ_{01} and $\Delta\mu = \mu_{11} - \mu_{00}$, respectively) of the investigated systems.[3,21,53]

In general, a consistent finding across various studies is that TD-DFT methods tend to underestimate the magnitudes of σ^{2PA}.[3,50,53,54] The accuracy of σ^{2PA} depends on the

precise calculation of ΔE and the 2PA transition strength (δ^{2PA}), which correspond to a transition from the ground state (S_0) to a higher excited state (S_n). The limitations of these calculations could be attributed to the constraints in charge transfer and the underestimation of the excited state dipole moments (μ_{11}),[19,36] where even in conjunction with accurate ground state dipole moments (μ_{00}), result in an underestimated permanent dipole moment change ($\Delta\mu$).[52] Thus, to obtain reliable σ^{2PA} values, it is essential that these properties are computed accurately. This reliability is evaluated through the exploration of unexplored functionals, which progress through the hierarchy from local density approximation (LDA), generalized gradient approximation (GGA), hybrid-GGA (H-GGA), RSH-GGA, meta-GGA (M-GGA), and hybrid M-GGA (HM-GGA), where the selection of methods is dependent on their availability in TURBOMOLE.[55,56] In this evaluation, the results obtained using the WFT method, RI-CC2, are chosen as a reference.

We have selected a series of coumarin derivatives, see Figure 1, which are commercially exploited for their tuned fluorescent properties. For example, they are used in a broad range of applications, such as cellular staining procedures,[57,58] fluorescence probes,[59,60] and

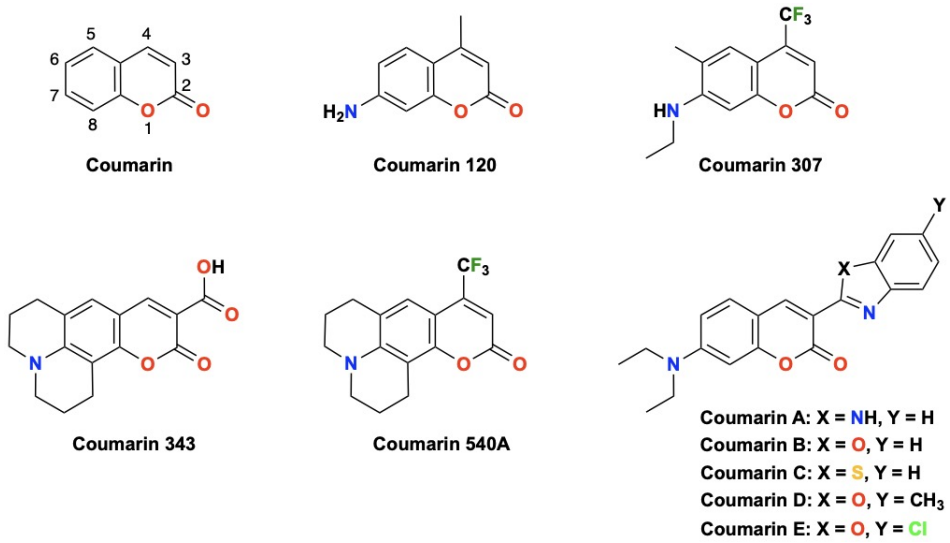

Figure 1: Coumarin dyes studied in this work.

sensitizers within solar cell technologies.[61,62] The selected coumarins are characterized by an electron-donating group (EDG), which is an amino substituent at position 7, paired with an electron-withdrawing group (EWG) at positions 3 or 4. The EWGs at position 3 include a carboxylic acid in coumarin 343, benzimidazolyl in coumarin A, benzoxazolyl in coumarins B, D, and E, or benzothiazolyl in coumarin C. Meanwhile, coumarins 307 and 540A feature a trifluoromethyl group at position 4 as their EDG. The selected derivatives are examples of donor–acceptor (D–A) dyes,[63] which support enhanced electron delocalization along their π-conjugated frameworks, a process that is further facilitated by stabilization from the aromatic rings.[23] Furthermore, the incorporation of D–A motifs facilitates the development of fluorescent low-lying excited states. This D–A arrangement results in a significant change in $\Delta\mu$, which impacts the values of $\sigma^{2\mathrm{PA}}$.[42]

1.1 Benchmarks of 2PA Cross-Sections, $\sigma^{\mathbf{2PA}}$. Previous benchmarks targeting $\sigma^{2\mathrm{PA}}$ have been somewhat limited to a relatively small array of functionals.[26,35,36,41,42,50–52,64] This approach is often characterized by the use of the 2-state model (2SM), which represents a sum-over-states approach considering transitions from S_0 to S_1. However, our investigation focuses on examining the results of quadratic response theory. Salem and Brown[50] provided a comparative analysis of the photophysical properties of isolated fluorescent protein (FP) chromophores using GAMESS[65] with five computational methods: H-GGA (PBE0 and B3LYP), RSH-GGA (CAM-B3LYP and LC-BLYP), and as implemented in Dalton,[66] WFT (CC2), utilizing the 6-31+G(d,p) basis set. The work involved comparing computed values of ΔE and $\sigma^{2\mathrm{PA}}$ with experimental data, while considering the limitations of such comparisons: ΔE values are indicative of vertical excitations, excluding vibronic effects or ground to excited state 0-0 transitions.[30,67] Furthermore, the comparison of $\sigma^{2\mathrm{PA}}$ with experimental values is limited by computational restrictions, such as the selected chromophore models,[37,68] environmental factors,[54,69] selected lineshape spectral broadening function, and conversion

to macroscopic GM units.[36] Overall, while ΔE values were relatively close across different functionals, the values of σ^{2PA} varied, particularly for higher-lying excited states. Moreover, values of σ^{2PA} obtained using TD-DFT were generally underestimated, compared to both CC2 calculations and experimental measurements. This underestimation of TD-DFT results has also been observed and discussed in later studies.[35,36,42,52,64] Beerepoot et al.[36] analysed FP chromophores using TURBOMOLE and Dalton by RI-CC2 and CAM-B3LYP, respectively, in conjunction with the aug-cc-pVDZ, aug-cc-pVTZ, and 6-31+G(d) basis sets. Their results suggest that the small computed values of σ^{2PA} are due to the underestimation of the computed μ_{11} values by CAM-B3LYP. Moreover, their work compares the obtained results to a previous benchmark[64] of equation-of-motion excitation energies coupled-cluster with single and double substitutions (EOM-EE-CCSD) results (implemented in Q-Chem),[70] where they found that their RI-CC2 values of σ^{2PA} are generally larger than EOM-EE-CCSD values by a factor that does not exceed 1.4.[36]

In another investigation focusing on isolated FP chromophores distinguished by their formal charge, either anionic or neutral, different DFT functionals were examined based on the percentage of HF exchange (E_x) they incorporate: GGA (BLYP), H-GGA (B1LYP, B3LYP, and BHandHLYP), and RSH-GGA (CAM-B3LYP).[52] These computations involved using GAMESS for TD-DFT analyses and TURBOMOLE for RI-CC2. For neutral FP chromophores, the computational predictions are sensitive to the E_x percentage; the lower the percentage, the greater the tendency to overestimate ΔE and exhibit larger discrepancies in σ^{2PA}. In contrast, calculations of σ^{2PA} values for anionic chromophores were more reasonable, due to their larger μ_{11} that influence $\Delta\mu$ upon excitation. Alternatively, the implementation of the second-order approximation time-dependent tight binding density functional theory (TD-DFTB2) within DFTB+,[71] which offers a less computationally demanding alternative, was applied to analyze the 2PA properties within the 2SM of 42 FP chromophores.[51] This approach, however, displayed limitations, including the underestimation and inconsistency

in trends of σ^{2PA} values, particularly when compared with results from B3LYP/6-31+G(d,p) and CAM-B3LYP/6-31+G(d,p). The observed discrepancies could be attributed to an overestimation of μ_{11}, contrasting with the previously determined underestimations in TD-DFT when compared with RI-CC2 results.[36] An alternative approach, simplified TD-DFT (sTD-DFT), has been employed in stda using sCAM-B3LYP/6-31+G(d) for FP and organic chromophores.[26] This method yields 2PA intensities that show relative improvement over the results from TD-DFT (CAM-B3LYP). However, challenges in accurately computing σ^{2PA} are still persistent.

Additional benchmarks have been established for the 2PA properties of relatively large organic molecules.[41,42] Beerepoot et al.[36] investigated organoboron chelates, utilizing both GAMESS and TURBOMOLE for the analysis. This study focused on the efficacy of six functionals, GGA (PBE and BLYP), H-GGA (B3LYP and PBE0), and RSH-GGA (CAM-B3LYP and LC-BLYP), with RI-CC2 serving as the reference, which they found to agree with existing experimental findings. The aug-cc-pVDZ basis sets were employed for these calculations, except for two systems where diffuse functions were omitted. Similar to previous findings,[41,50,52] these functionals typically underestimate δ^{2PA} (on which they base their analysis), and consequently σ^{2PA}, by a factor between 2 and 6; see Section 2 for the relationship between δ^{2PA} and σ^{2PA}. The observed discrepancies can primarily be attributed to a slight underestimation of μ_{11} and a marginal overestimation of ΔE. In contrast, among the evaluated functionals, RSH-GGAs show a qualitative agreement with both experimental data and RI-CC2 results, particularly in accurately predicting the order of δ^{2PA}. Complementing this analysis, a recent investigation by the same research group,[42] encompassing an extensive set of 48 organic compounds featuring D–A groups and utilizing similar computational approaches, further supports these findings. However, their recent work,[42] employing the aug-cc-pVDZ basis set, indicates that while RSH-GGA functionals correlate closely with RI-CC2 outcomes, the H-GGA methods perform somewhat better in calculating the magni-

tudes of δ^{2PA}.[42] Furthermore, a recent investigation has explored this set of 48 π-conjugated systems using various functionals, including M-GGA and HM-GGA, in conjunction with the Def2-SVPD basis set through VeloxChem.[72,73] However, the investigation predominantly concentrates on the δ^{2PA} values rather than the experimentally measurable parameter σ^{2PA},[73] where the analysis is similar to the previous work of Chołuj et al.[42] Examples, based on the present work, showing the potential inconsistencies in the evaluation of functionals based on δ^{2PA} values as opposed to σ^{2PA} values are outlined Section 3.2.1. Moreover, the investigation of Ahmadzadeh et al.[73] demonstrates that functionals such as M06-2X, MN15, M05-2X, CAM-B3LYP, MPWB1K, and BB1K, among others, display comparable correlations with RI-CC2, each exceeding 0.98 in correlation coefficients with low mean relative errors. However, the values of $\Delta\mu$ remain rather underestimated.

Recent explorations into models of cationic rhodopsin chromophores, employing widely-used GGA functionals (BLYP), H-GGA (B1LYP, B3LYP, and BHandHLYP), and RSH-GGA (CAM-B3LYP), and comparing them with higher-order correlated WFT methods like CCSD, CC2, and CC3, have shed light on the errors associated with WFT in computing σ^{2PA}.[35] The findings indicate that the use of CC2/aug-cc-pVDZ results in deviations of merely 2%, relative to CCSD and CC3, whose results are somewhat similar. This small deviation is in contrast to the 10% difference observed when using CC2/6-31+G(d). It is worth noting that their computational analyses have been performed using Dalton, which does not incorporate the resolution-of-identity approximation. Alternatively, when considering DFT functionals, it was observed that CAM-B3LYP and BHandHLYP showed a good correlation with the reference data, despite considerable inaccuracies in predicting absolute 2PA intensities.

Explored benchmarks have consistently identified RSH-GGA methods, particularly the CAM-B3LYP/aug-cc-pVDZ level of theory, as preferred for 2PA calculations. However, these benchmarks also revealed a consistent trend of underestimation in the calculated σ^{2PA} and μ_{11} values. Moreover, while certain functionals have been frequently utilized, there

remains a number of functionals that have yet to be investigated. Therefore, it becomes imperative to expand the range of explored functionals to find a method that not only balances these properties effectively but potentially surpasses the performance of CAM-B3LYP in these calculations. The scope of this research encompasses a thorough analysis of various E_{xc} functionals, as categorized by Jacob's Ladder hierarchy, to evaluate their efficacy in determining σ^{2PA} and μ, as well as their correlation with RI-CC2 benchmarks. The computations and analysis particularly focus on previously unexplored methods within quadratic response theory and also include the use of the quantum theory project (QTP) functionals, CAM-QTP-00,[74] CAM-QTP-01,[75] CAM-QTP-02,[76] and LC-QTP,[76] which, as they were developed through rigorous correlated orbital theory arguments,[77] mitigate the devil's triangle of errors present in Kohn–Sham DFT.[78]

2 Computational Methods

The geometry optimization of the selected coumarin dyes was performed using Gaussian16,[79] utilizing the B3LYP[80,81] functional alongside the D3 dispersion correction with Becke-Johnson (BJ) damping.[82–85] The geometries were confirmed as minima by evaluating the vibrational frequencies, which showed no imaginary frequencies. The electronic excitation processes in this work involved transitions from the singlet ground state, S_0, to the first singlet excited state, S_1. To compute these excitations, response theory was applied using TD-DFT[40,86] and WFT (RI-CC2),[39] utilizing TURBOMOLE.[55,56] However, the LC-QTP excitation calculations were performed using Dalton,[66] since LC-QTP is not implemented in TURBOMOLE. All computational tasks, ranging from geometry optimization to the calculations of the excited states, were carried out in the gas phase using the aug-cc-pVDZ basis set.[87,88] This basis set has proven to be sufficient for 2PA intensity calculations.[42,52] For 2PA calculations, the assumption of linearly polarized light was used.

To obtain the value of σ^{2PA} in macroscopic units, the following expression is used,

$$\sigma^{\mathrm{2PA}} = \frac{N\pi^2 a_0^5 \alpha \omega^2}{c\Gamma}\delta^{2PA} \tag{1}$$

where the parameters are defined as follows: $N = 4$ is an integer; a_0 is the Bohr radius; α is the fine-structure constant; ω, is the photon energy (derived from $\frac{\Delta \mathrm{E}}{2}$); c is the speed of light; and Γ, is the lifetime broadening, which is set to 0.1 eV. However, the transition strength term, δ^{2PA}, varies based on the computational approach used, either TD-DFT or RI-CC2. In the case of TD-DFT, δ^{2PA} is expressed as follows,

$$\delta^{\mathrm{2PA}} = \frac{1}{15}\sum_{\alpha\beta}[S_{\alpha\alpha}S^*_{\beta\beta} + 2S_{\alpha\beta}S^*_{\alpha\beta}] \tag{2}$$

where $S_{\alpha\beta}$ $(\alpha, \beta = x, y, z)$ is the two-photon transition matrix element, which is formulated as,

$$S_{\alpha\beta} = \sum_n \left[\frac{\langle 0|\mu_\alpha|n\rangle\ \langle n|\mu_\beta|f\rangle}{\omega_n - \omega_1} + \frac{\langle 0|\mu_\beta|n\rangle\ \langle n|\mu_\alpha|f\rangle}{\omega_n - \omega_2}\right]. \tag{3}$$

In Eq. 3, $\mu_{\alpha,\beta}$ is the Cartesian dipole moment component and ω_n is the excited state energy represented by excitation from $|0\rangle$ to an intermediate state $|n\rangle$.

With RI-CC2, the approach involves a Jacobian non-symmetric matrix ($\mathcal{A}$), leading to distinct left ($\mathcal{L}$) and right ($\mathcal{R}$) eigenvectors. Consequently, when calculating $S_{\alpha\beta}$, it becomes necessary to use both these eigenvectors, resulting in a unique expression for δ^{2PA}, presented as,

$$\delta^{\mathrm{2PA}}_{0f} = \frac{1}{15}\sum_\alpha\sum_\beta\left[S^{\alpha\alpha}_{f\leftarrow 0}S^{\beta\beta}_{0\leftarrow f} + S^{\alpha\beta}_{f\leftarrow 0}S^{\alpha\beta}_{0\leftarrow f} + S^{\alpha\beta}_{f\leftarrow 0}S^{\beta\alpha}_{0\leftarrow f}\right] \quad \alpha, \beta \in x, y, z \tag{4}$$

where $S^{\alpha\alpha}_{f\leftarrow 0}$ and $S^{\beta\beta}_{0\leftarrow f}$ denote the left and right components of $S_{\alpha\beta}$, respectively. Defined in

terms of Cartesian coordinates, their expressions are,

$$S^{\mathcal{L}}_{xy} = S^{xy}_{0\leftarrow f} = \sum_n \left[\frac{\langle 0|\mu_x|n\rangle \ \langle n|\mu_y|f\rangle}{\omega_n - \omega_1} + \frac{\langle 0|\mu_y|n\rangle \ \langle n|\mu_x|f\rangle}{\omega_n - \omega_2} \right] \tag{5}$$

$$S^{\mathcal{R}}_{xy} = S^{xy}_{f\leftarrow 0} = \sum_n \left[\frac{\langle f|\mu_x|n\rangle \ \langle n|\mu_y|0\rangle}{\omega_n - \omega_1} + \frac{\langle f|\mu_y|n\rangle \ \langle n|\mu_x|0\rangle}{\omega_n - \omega_2} \right]. \tag{6}$$

The excitation energy in RI-CC2 is determined using the following relation,[89,90]

$$\left[\mathcal{A}_{1,1} - \frac{\mathcal{A}_{1,2}\mathcal{A}_{2,1}}{\varepsilon_2 - \omega} \right] \mathcal{R}_1 = \omega \mathcal{R}_1, \tag{7}$$

$$\mathcal{R}_2 = -\frac{\mathcal{A}_{2,1}\mathcal{R}_1}{\varepsilon_2 - \omega} \tag{8}$$

where indexes 1 and 2 represent the terms arising from single and double excitations, respectively.

Overall, a total of 19 E_{xc} functionals were selected to compute σ^{2PA} and μ for the chosen dyes. Moving through the rungs of Jacob's ladder, the methods included LDA (S-VWN[91,92]), GGA (PBE[93]), H-GGA (BHandHLYP,[94–96] B3LYP,[94–97] PBE0[98]), RSH-GGA (CAM-B3LYP,[99] CAM-QTP-00,[74] CAM-QTP-01,[75] CAM-QTP-02,[76] LC-QTP,[76] ωB97X,[100] ωB97X-V,[101] LRC-ωPBEh[102]), M-GGA (TPSS[103]), and HM-GGA (M11,[104] M06,[105] M06-2X,[105] M06-L,[106] TPSSh[107]). This work applies response theory to analyze RSH-GGA (excluding CAM-B3LYP), M-GGA, and HM-GGA functionals (many for the first time for any system), examining the computed values of 2PA intensities and observed trends therein. It is worth noting that to enhance the clarity of the Figures, some plots discussed in the manuscript do not include the results for certain methods, however, these are provided in the SI. Moreover, all numerical values of the investigated photophysical parameters are tabulated in the SI.

3 Results and discussion

3.1 Excitation Energies, ΔE. This work briefly addresses values of ΔE for the excitation from S_0 to S_1 because they have been extensively investigated and discussed for various systems.[29–31,48–50,67,108] The computed ΔE, mean absolute error (MAE), mean signed error (MSE), and % error values at different levels of theory are provided in Tables S1−S4. In agreement with earlier studies,[50,67] our results indicate that functionals like PBE0 and M06 are closely comparable to RI-CC2, which is demonstrated by the lowest MAE values of 0.06 and 0.08 eV, respectively, see Figure 2. In contrast, other functionals exhibit MAE with values exceeding 0.10 eV, with no clear trend in overestimation or underestimation of computed values. In particular, functionals including BHandHLYP, M11, M06-2X, and RSH-GGA show a tendency to overestimate ΔE, see Figure S31. In CAM-B3LYP, this trend is moderated, while a contrasting trend of underestimation is observed in PBE0, M06, and B3LYP. However, these functionals produce values that align relatively closer with RI-CC2, generally within a margin of 0.10 eV or less (Table S3 and Figure S31). On the other hand, functionals like S-VWN, PBE, TPSS, M06-L, and TPSSh underestimate ΔE values by more than 0.20 eV, based on their calculated MSE values. It is important to note that the efficacy of these functionals varies depending on the specific system and its formal charge. For example, CAM-B3LYP generally underestimates ΔE (relative to RI-CC2) for anionic chromophores while showing consistency for neutral chromophores,[52] which is in agreement with the results obtained herein where ΔE values obtained using CAM-B3LYP are generally within 0.10 eV, compared to RI-CC2 values.

In terms of reproducing qualitative trends, functionals like S-VWN, B3LYP, and TPSSh do not replicate the dyes ranking of ΔE as observed in RI-CC2, showing the importance of cautious interpretation when using these functionals for qualitative analysis of ΔE, particularly when environmental conditions such solvent interactions are involved.[37,109] Overall,

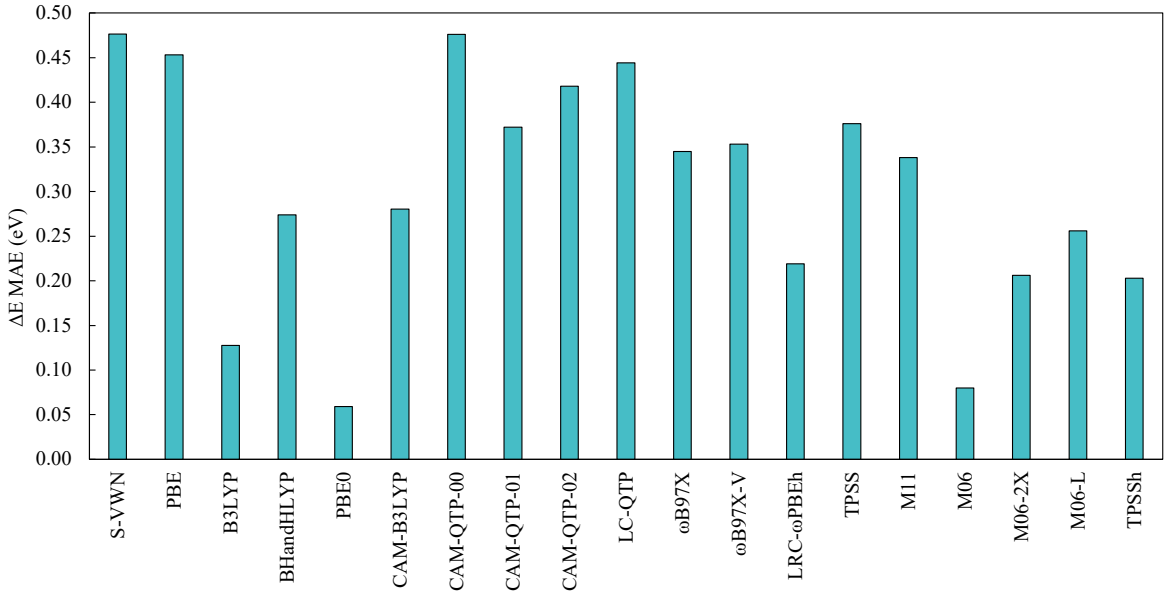

Figure 2: MAE of ΔE (eV) for the **coumarin dyes** in reference to RI-CC2/aug-cc-pVDZ values.

both quantitative and qualitative accuracy of excited state results is substantially dependent on the selected functional, which is due to the fact that these functionals are parameterized and fine-tuned with a focus on ground state properties.

3.2 Which Functional to Choose for $\sigma^{\mathbf{2PA}}$ Calculations? The computational determination of 2PA intensities has prioritized qualitative insights,[37] primarily due to the challenges in quantification of $\sigma^{2\mathrm{PA}}$ and precise calculation of molecular properties such as μ_{00}, μ_{01}, and μ_{11}.[36,50] This qualitative prioritization is evident in the typically lower $\sigma^{2\mathrm{PA}}$ values derived from TD-DFT compared to those from experimental data and wavefunction-based methods.[42,52,64,69] Consequently, while TD-DFT tends to underestimate values of $\sigma^{2\mathrm{PA}}$, this work emphasizes the relative magnitudes and trends yielded by TD-DFT as compared to RI-CC2, to evaluate the efficacy of the selected functionals in predicting $\sigma^{2\mathrm{PA}}$. It should be noted that the focus of this work has been placed predominantly on the values of $\sigma^{2\mathrm{PA}}$ over $\delta^{2\mathrm{PA}}$, as the former represents the parameter that is experimentally observed and re-

ported.[21] It should be noted that the comparative assessment of MAEs of σ^{2PA} and δ^{2PA} does not yield similar qualitative results, as depicted in Figure 3 and in Tables 1 (σ^{2PA}) and S6 (δ^{2PA}). Furthermore, the study involves categorizing the evaluated functionals according to their computed MAEs. While minimal discrepancies are noted in certain instances, this ranking approach facilitates a structured and clear presentation of the results, thereby enabling a more systematic comparison and tabulation of the findings. The calculated photophysical properties, including σ^{2PA}, ΔE, μ_{00}, μ_{11}, μ_{01}, and $\Delta\mu$, are provided in Table S1, their MAEs in Table S2, MSEs in Table S3, and % errors in Table S4. These data are graphically represented across Figures S1 to S38 in the SI, whereas the linear regression data from correlating TD-DFT with RI-CC2 are depicted in Figures S39 to S57, covering all investigated dyes. To provide a comprehensive overview of computed 2PA parameters, the δ^{2PA} values as well as their corresponding MAEs, MSEs, and % errors are detailed in Table S5, and the results of their linear regression analysis are provided in Table S6. The ranking of functionals based on MAEs of their computed μ_{01}, μ_{00}, μ_{11}, and $\Delta\mu$ values is available in Table S7. It should be noted that the analysis of functionals and discussion presented herein is based on the calculated MAEs, which provide similar qualitative insights to both MSEs and % errors.

3.2.1 Analysis Based on MAEs of σ^{2PA}. The range of MAEs for the functionals varies significantly with variations reaching 38.00 GM, see Figure 3, which indicates substantial differences in the accuracy of DFT functionals for σ^{2PA}. The variation in the MAEs between functionals spans from modest, 0.20 GM, to more substantial differences, 8.00 GM. Generally, the RSH-GGA methods exhibit a distinguishable performance, yet it is the M11, M06-2X, ωB97X, and QTP variants, that stand out with their efficacy. In particular, M11, along with LC-QTP, CAM-QTP-02, and CAM-QTP-01, yield the lowest MAEs among the functionals, which is a result of their parameterization as well as their ability to capture both short-

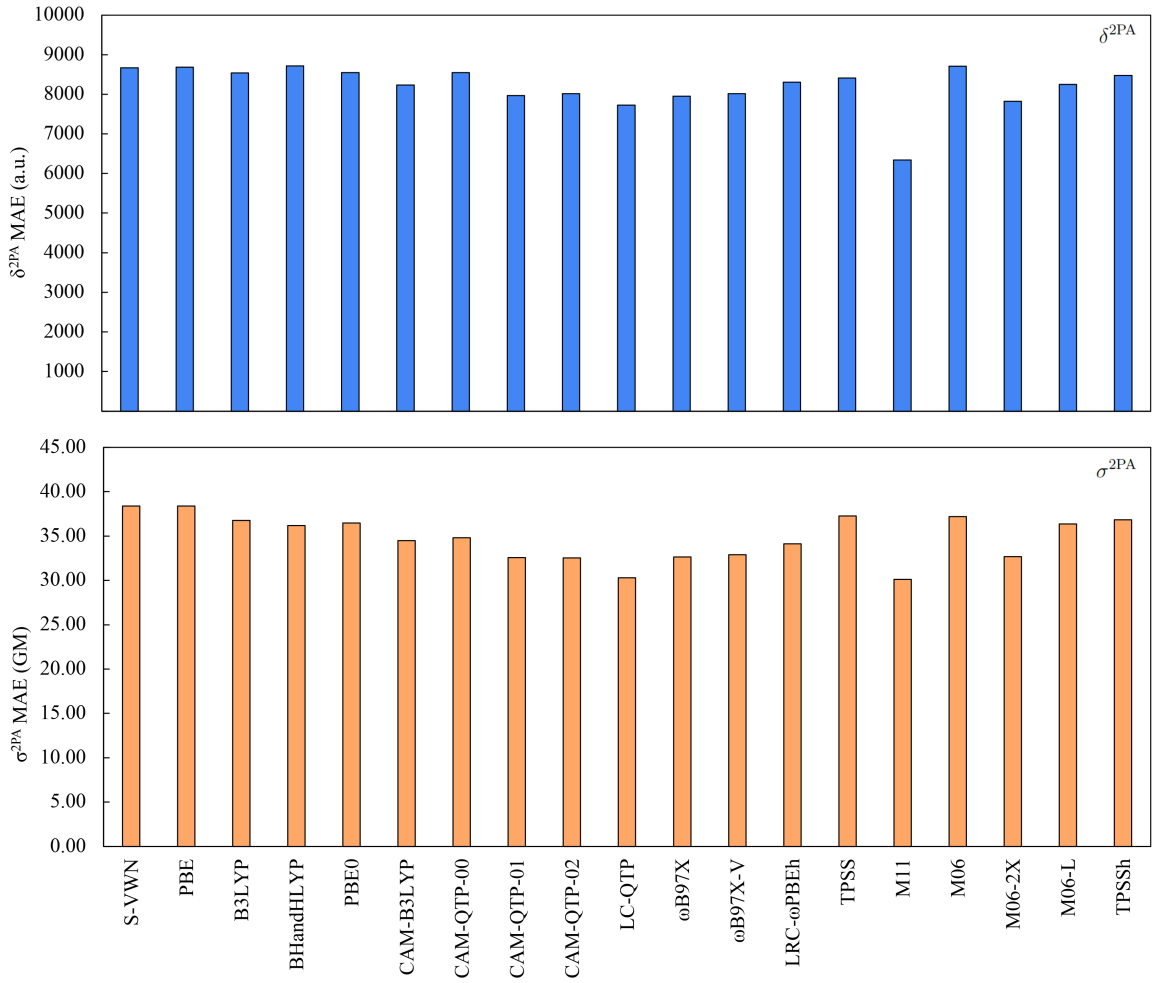

Figure 3: MAE of σ^{2PA} (GM) and δ^{2PA} (a.u.) for the **coumarin dyes** in reference to RI-CC2/aug-cc-pVDZ values.

range (SR) and long-range (LR) electron correlation effects. The QTP variants have not previously been considered for σ^{2PA} and show promising results. Accordingly, it is essential to understand how these variants rank relative to other functionals, in terms of their MAE. Similar to previous findings,[36,41,50,52] the computed σ^{2PA} values are underestimated by at least 30 GM, see Table S3 and Figure S32.

In the assessment of functionals based on their MAEs, the following hierarchy emerges: M11 leads, closely followed by LC-QTP, and succeeded by CAM-QTP-02, CAM-QTP-01, ωB97X, M06-2X, ωB97X-V, and LRC-ωPBEh, see Table 1. Other notable functionals in-

clude CAM-B3LYP, CAM-QTP-00, and BHandHLYP, proceeding to PBE at the lower end. Intriguingly, the top eight functionals, showcasing the lowest MAEs, have not previously been reported (except for the recently reported M06-2X and TPSSh)[73,110] for σ^{2PA} computations. Particularly, M11, three QTP variants, ωB97X, and M06-2X ranking among these top functionals, highlight the significance of considering both short-range (SR) and long-range (LR) E_{xc} effects, as well as the Hartree-Fock E_x exchange percentage, in influencing the accuracy of computed values. Thus, the results are analyzed based on the SR, LR, and HF E_x percentage, where these percentages are provided in Table 1.

The integration of both SR and LR corrections lowers the observed MAEs, which is especially apparent in functionals where a somewhat balanced mix of SR and a complete 100% LR correction is implemented. Such functionals, including M11, LC-QTP, ωB97X,

Table 1: MAEs of σ^{2PA} (GM) and linear regression data from correlating TD-DFT with RI-CC2.

Rank[†]	Functional	% HF E_x	σ^{2PA} MAE	m	b	R^2
1	M11	42.8–100	30.10	3.5404	-0.6983	0.960
2	LC-QTP	0–100	30.30	3.6057	-0.7584	0.920
3	CAM-QTP-02	28–72	32.54	3.7823	5.5908	0.755
4	CAM-QTP-01	23–77	32.57	3.8306	5.2239	0.773
5	ωB97X	15.77–100	32.63	3.9354	4.471	0.806
6	M06-2X	54	32.69	3.2218	11.5	0.642
7	ωB97X-V	16.7–100	32.89	3.9786	5.1029	0.788
8	LRC-ωPBEh	20–100	34.11	3.6931	12.255	0.619
9	CAM-B3LYP	19–65	34.47	3.0657	18.457	0.450
10	CAM-QTP-00	54–91	34.81	2.9111	20.638	0.388
11	BHandHLYP	50	36.18	1.2871	34.448	0.087
12	M06-L	0	36.36	-0.9286	47.666	0.043
13	PBE0	25	36.46	0.7273	38.03	0.024
14	B3LYP	20	36.75	0.0899	41.731	0.0004
15	TPSSh	10	36.83	-0.4357	44.575	0.008
16	M06	27	37.19	-0.2093	43.277	0.002
17	TPSS	0	37.27	-1.1277	47.807	0.048
18	S-VWN	0	38.38	-1.9762	49.816	0.090
19	PBE	0	38.40	-2.1047	50.267	0.118

[†]Ranking of functionals is based on MAEs.

ωB97X-V, and LRC-ωPBEh, have emerged as leading ones in our analysis. LC-QTP, however, is an exceptional case among these functionals. It is unique in using a 0% SR and a full 100% LR correction, yet it yields results that are comparable to M11, which has a significant SR component (42.8%). Moreover, LC-QTP even outperforms ωB97X (SR = 15.77%), ωB97X-V (SR = 16.7%), and LRC-ωPBEh (SR = 20%). This performance is due to the special parameterization of the QTP variants, which are tuned for excited state properties that significantly influence them.[78] This performance is evident as CAM-QTP-00 ($54-91\%$), CAM-QTP-01 ($23-77\%$), and CAM-QTP-02 ($28-72\%$) all demonstrate effective outcomes. While CAM-QTP-02 exhibits a higher proportion of SR (28%) and a lower LR (72%) compared to CAM-QTP-01 ($23-77\%$), and indicates smaller proportions of both SR and LR compared to CAM-QTP-00 ($54-91\%$), it slightly surpasses them in performance. However, the difference in performance of CAM-QTP-02 to CAM-QTP-01 is minor, with negligible variation in MAEs and absolute values of $\sigma^{2\mathrm{PA}}$; a reasonable outcome considering the slight difference in their SR and LR contributions. While it is crucial to emphasize that CAM-QTP-02 completely obeys the correlated orbital theory arguments by satisfying both the ionization potential and electron affinity conditions, it differs from CAM-QTP-01, which only incorporates the ionization potential condition.

Interestingly, despite its prevalent use, the CAM-B3LYP functional demonstrates a less favourable performance in our analysis, positioned at 9^{th} in the MAE ranking. This functional shows an MAE 4.37 GM higher than that of M11, which exhibited the lowest MAE. This variance, albeit slight, indicates the potential impact exerted by the specific systems selected for this study on the relative performance of the investigated functionals. The impact of the selected system's characteristics on the MAE becomes particularly evident in cases where $\sigma^{2\mathrm{PA}}$ values are significant, exceeding 100 GM. A particular illustration of this is coumarin E, which has the largest $\sigma^{2\mathrm{PA}}$ value according to RI-CC2 calculations, see Table S1. In this case, the MAE for CAM-B3LYP shows a notable difference from M11, reaching

9.76 GM. In contrast, when analyzing systems with lower σ^{2PA} values, such as coumarin 120, the observed difference in MAE between CAM-B3LYP and M11 is considerably diminished to a narrow difference of 0.50 GM. While the numerical differences in MAE among various functionals may appear minimal, the identification of the functional with the lowest MAE is important. This significance stems from the dependency on the magnitude of the computed σ^{2PA}, generally below 70 GM for the studied dyes. It is worth noting that functionals yielding the lowest MAE for σ^{2PA} do not necessarily coincide with those exhibiting the lowest MAE for ΔE.

Further analysis reveals that functionals, excluding RSHs, appear to be partially influenced by their incorporated percentage of HF E_x, where a proportion higher than 50% tends to yield lower MAE values, in agreement with observations reported previously.[52] On the contrary, in the case of functionals where the HF E_x is less than 50%, the resulting MAEs are higher, even though the differences in MAEs across these functionals are relatively small. However, an exception is observed in the case of Minnesota functionals. These functionals excel, outperforming their counterparts, due to their HF E_x percentage and relatively reliable predictions of charge transfer.[111–113] A clear illustration of this independence from HF E_x is observed in the comparison between M06-L and M06, where the former, with 0% E_x, somewhat outperforms the latter, which has a 27% E_x. This aspect sets the Minnesota functionals apart from others in terms of performance efficiency. The lower errors observed in Minnesota functionals were previously reported for both MN15 (not used herein) and M06-2X in 2SM[42] and response theory 2PA calculations.[73,110] Alternatively, functionals such as BHandHLYP, PBE0, B3LYP, TPSSh, TPSS, S-VWN, and PBE, each with an HF E_x of 50% or lower, are associated with higher MAEs in comparison to RSHs, highlighting their dependence on the E_x percentage. For instance, BHandHLYP, having a 50% E_x , occupies the 11^{th} rank, while PBE0 ($E_x = 25\%$), B3LYP ($E_x = 20\%$), and TPSSh ($E_x = 10\%$) rank as 13^{th}, 14^{th}, and 15^{th}, respectively, see Figure 3. The ranking of BHandHLYP, PBE0, and B3LYP between 11^{th}

and 15$^{\text{th}}$ positions in our list of functionals contrasts with previous findings,[41,42,114] which indicated their efficiency in calculating 2PA intensities in dyes, particularly those with D–A moieties[42] and in other organic dyes.[41,114] However, the observed discrepancy between our findings and previous studies is attributed to the limited range of functionals explored in those earlier investigations.[41,42,50,52] Moreover, our analysis finds that functionals with no E_x component, specifically TPSS, S-VWN, and PBE, are associated with the highest MAEs, placing them at a performance level towards the lower end.

Overall, our results indicate that functionals such as the Minnesota and QTP variants, along with ωB97X, are effective for calculating $\sigma^{2\text{PA}}$, with M11 and LC-QTP being particularly recommended. In the rung of RSH-GGA methods, functionals that tend to balance SR and LR corrections exhibit superior performance compared to CAM-B3LYP, and occasionally even surpass other functionals. On the other hand, local functionals with no E_x are not suitable for such calculations.

3.2.2 Analysis Based on Linear Regression of $\sigma^{2\text{PA}}$ Between TD-DFT and RI-CC2.

The focus of this work is to identify functionals aligning well in terms of both quantitative and qualitative analyses of $\sigma^{2\text{PA}}$, rather than to engage in an exact quantitative comparison of functionals, considering the small differences in R^2 values observed between some of the functionals, *e.g.*, CAM-QTP-01 and CAM-QTP-02. The largest linear regression, R^2, values are associated with functionals that have a broad range of SR, LR, and HF E_x, implying that a balanced approach to the inclusion of such correlation effects is beneficial for reliable $\sigma^{2\text{PA}}$ predictions. However, similar to the previous analysis, the data does not support a linear relationship between the exchange percentage included and predictive functional accuracy, as seen by the varied R^2 values (Table 1).

Functionals exhibiting the lowest MAEs also tend to display the highest R^2 values, indicating reliable quantitative and qualitative performance. This correlation is evident in

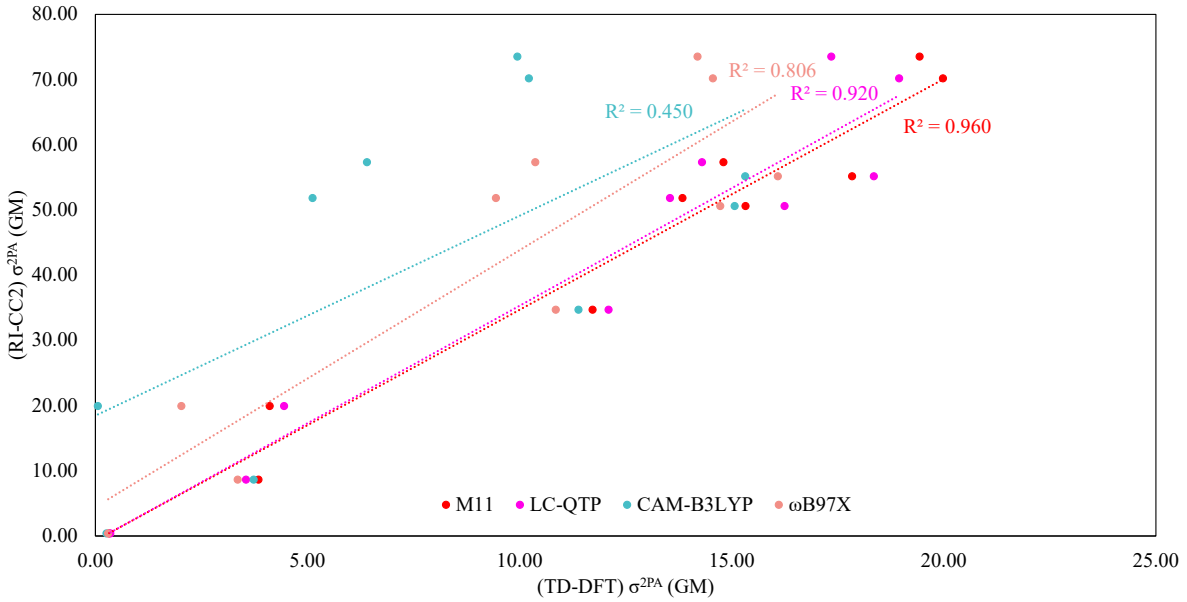

Figure 4: Linear regression analysis of σ^{2PA} comparing TD-DFT functionals with largest R^2 values versus RI-CC2. CAM-B3LYP is included for benchmarking purposes.

the case of M11, which has an R^2 of 0.960, and LC-QTP, with an R^2 of 0.920 (Figure 4), showing their relative reliability in σ^{2PA} calculations. However, there is a partial inconsistency observed between the rankings based on R^2 values and MAEs. For instance, ωB97X, which exhibits a higher R^2 value of 0.806 compared to CAM-QTP-01 ($R^2 = 0.773$) and CAM-QTP-02 ($R^2 = 0.755$), is associated with a minimally larger MAE. A similar pattern is noted with M06-2X and ωB97X, where the former has an R^2 of 0.642, significantly lower than the latter's 0.788, yet it demonstrates a comparable performance based on MAE. Following these, comes LRC-ωPBEh with an R^2 of 0.619, still demonstrating a reasonable R^2. These observations reveal that the top 9 functionals not only have the largest R^2 values but also exhibit the smallest MAEs, relative to RI-CC2 results.

Despite the widespread use of CAM-B3LYP in such σ^{2PA} computations, its R^2 value of 0.450, as detailed in Figure 4, is notably lower than expected when compared to other functionals. Previous research,[42] which is based on evaluating δ^{2PA} values, has indicated that CAM-B3LYP, along with B3LYP and PBE0, can yield R^2 values ranging from 0.85

to 0.99 for a different set of organic systems.[42] Furthermore, it has reported that PBE, B3LYP, and PBE0 can produce 2PA intensities exceeding those from RI-CC2,[42] a unique finding suggesting that certain TD-DFT methods can surpass RI-CC2 results. However, it is crucial to acknowledge that the analysis of Chołuj et al.[42] primarily concentrated on analyzing R^2 values of δ^{2PA} reported in atomic units, rather than σ^{2PA} defined in GM, which potentially leads to different findings. This difference can be confirmed by taking examining the expressed R^2 results herein in terms of δ^{2PA} instead of σ^{2PA}, which potentially leads to different qualitative insights, see Table S6. This difference arises because σ^{2PA} also incorporates any differences in ΔE (*i.e.*, ω) values, see Eq. 1.

In particular, the application of a linear regression approach to δ^{2PA} reveals a marked decrease in the effectiveness of both M11 and LRC-ωPBEh, contrasting with their superior performance in σ^{2PA}. Hence, the general results presented in benchmarks may be influenced by several factors, including the specific systems selected and their respective sizes, as well as 2PA parameters chosen for analysis, such as δ^{2PA} and σ^{2PA}. For example, if functionals predict that the values of δ^{2PA} are close to the RI-CC2 values, it does not necessarily mean that they are superior to others. This can be seen clearly in the work of Chołuj et al.,[42] where for molecules 43 and 46, predicted δ^{2PA} values of B3LYP (43 = 119546 and 46 = 265907 a.u.) and PBE0 (43 = 107108 and 46 = 236298 a.u.), based on their analysis, are the closest to RI-CC2 values (43 = 102475 and 46 = 242707 a.u.), and their values, at different levels of theory, are generally close to RI-CC2 ones. However, if values of molecules 43 and 46 from their work are converted to σ^{2PA}, using their computed ΔE in their SI, it will lead to B3LYP values of 43 = 313.64 and 46 = 597.62 GM and PBE0 values of 43 = 319.59 and 46 = 593.67 GM. These σ^{2PA} values differ by at least 150 GM from their RI-CC2 values of 43 = 469.58 and 46 = 784.00 GM, which would be the case for the rest of their system. Moreover, when considering values computed by other superior functionals as reported in their study,[42] CAM-B3LYP and LC-BLYP yield values of 43 = 52511 and 46 = 72815 a.u., and 43 = 30470

and 46 = 35088 a.u., respectively. These correspond to (CAM-B3LYP) 43 = 231.40 and 46 = 270.41 GM and (LC-BLYP) 43 = 157.62 and 46 = 150.55 GM, exhibiting a substantial discrepancy from RI-CC2 values of up to 633 GM. Such significant deviations not only diminish their reported high correlation coefficients but also alter their qualitative outcomes, similar to the changed ranking obtained herein in Tables 1 and S6. Much like Chołuj et al.,[42] the recent assessment conducted by Ahmadzadeh et al.[73] focuses on δ^{2PA} values, reinforcing the reliability of our examination of functionals and their corresponding σ^{2PA} values.

Overall, functionals with both SR and LR components such as M11, LC-QTP, ωB97X, CAM-QTP-01, and CAM-QTP-02 are observed to outperform others. On the other hand, functionals with HF $E_x \leq 50\%$, which result in R^2 values at or below 0.10, demonstrate a weak predictive ability in this regression model. This implies that TD-DFT calculations using these functionals ($E_x \leq 50\%$) are not as reliable for predicting σ^{2PA} values. The comprehensive analysis of functionals presented is substantiated by the results obtained from linear regression, as depicted in Figures 4 and S39 to S57, and MAEs detailed in Table 1.

3.2.3 Analysis of Dipole Moments, μ. Dipole moments, quantified as the product of charge magnitude and the distance between charges, elucidate the distribution of electron density in polar molecules. Their behavior under an external electric field provides valuable information about the molecule's electronic structure, polarity, and photophysical characteristics. While dipole moments are commonly calculated as indicators of electron density quality, reasonably accurate dipole moments can occasionally arise from inaccurate electron densities. Despite this issue, dipole moments remain fundamental observables that are sensitive to errors in density calculations. However, in this work, the evaluation of μ_{00}, μ_{11}, $\Delta\mu$, and μ_{01} goes beyond comparing magnitudes with RI-CC2 values. We aim to identify qualitative trends in functional behaviour, particularly in terms of underestimation or over-

estimation of these parameters, and examine their consistency with functionals providing relatively reliable $\sigma^{2\mathrm{PA}}$ computations. The significance of these dipole moments is manifested in their influence on $\delta^{2\mathrm{PA}}$ (Eq. 2) magnitudes via $S_{\alpha\beta}$ (Eq. 3 for TD-DFT), as well as in $\delta_{0f}^{2\mathrm{PA}}$ (Eq. 4 for RI-CC2), involving S_{xy}^{L} (Eq. 5) and S_{xy}^{R} (Eq. 6). Previous explorations in this domain include both experimental findings illustrating the role of $\Delta\mu$,[6,21] and computational studies employing the 2SM,[36,42,52,115] yet our focus is predominantly on the insights gained from response theory with the investigated functionals.

The selected functionals were analyzed for their performance in quantifying μ_{00}, μ_{11}, $\Delta\mu$, and μ_{01} of coumarins, listed in Tables S1− S4 and illustrated in Figures 5 and S34, relative to the RI-CC2 values. It was found that for transition dipole moments, μ_{01}, functionals generally underestimate these values, see Table S3 and Figure S34. Similarly, analysis of the excited state dipole moments, μ_{11}, shows a significant underestimation exceeding 2 Debye in the predicted values. This pattern indicates a possible systematic bias in the functionals' performance, particularly noticeable in dyes with larger computed magnitudes. A mix of overestimated and underestimated μ_{11} values has been observed in previous studies,[36,52] depending on the investigated systems. On the other hand, ground state dipole moments, μ_{00}, are overestimated. Moreover, functionals generally overestimate $\Delta\mu$ values, with the exception of LC-QTP, LRC-ωPBEh, and TPSS where they underestimate them (Figure S34). This observation contrasts with the recent findings of Ahmadzadeh et al.,[73] which suggest an underestimation in the magnitudes of $\Delta\mu$. Naturally, $\Delta\mu$ depends on values of both μ_{00} and μ_{11}, where errors in either could significantly affect the resulting values.[36,42] In addition to quantitative estimations, it is essential to examine MAEs associated with the dipole moments. This analysis aims to characterize these errors in relation to the computed values of $\sigma^{2\mathrm{PA}}$, thereby assessing whether investigated functionals replicate the qualitative trends observed in their performance when computing $\sigma^{2\mathrm{PA}}$. It is worth noting that the discussion emphasizes the examination of considerable discrepancies and the ranking of previously

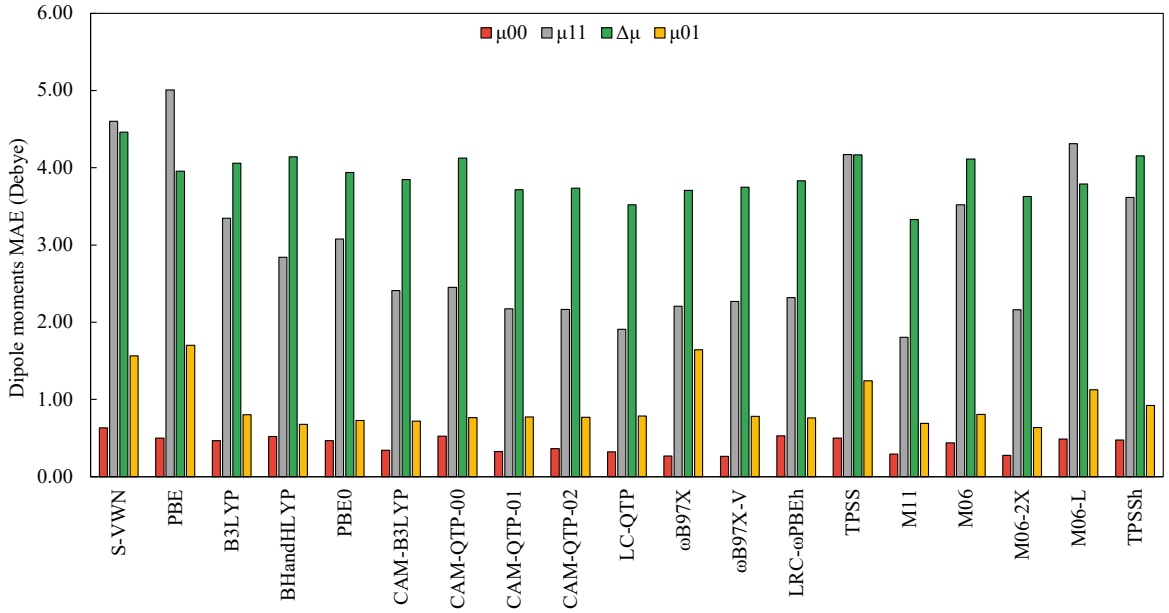

Figure 5: MAE of μ_{00}, μ_{11}, $\Delta\mu$, and μ_{01} (Debye) for the **coumarin dyes** in reference to RI-CC2/aug-cc-pVDZ values.

unexplored functionals in detail; the rest generally follows a similar trend and ranking in Table S6.

In general, it is evident that at least one or more functionals among the top nine, which excelled in σ^{2PA} computations, also achieved the lowest MAEs for one or more of the μ parameters (Figure 5). In particular, the RSH-GGA and HM-GGA functionals (mainly M11 and M06-2X) dominate the rankings, displaying a slight discrepancy in μ_{01} in some functionals. M06-2X emerges as the leading functional, achieving an MAE of 0.64, thereby showing its effectiveness in modeling electronic transitions. However, the aforementioned discrepancy is found in the superior performance of BHandHLYP, ranking after M06-2X with an MAE of 0.68, which is closely matched by M11 with an MAE of 0.69, as shown in Table S6. In a similar fashion to the discrepancy noted earlier, previously considered functionals such as CAM-B3LYP and PBE0 have also demonstrated superior performance, where these are the only discrepancies observed in the functional performance evaluation. Such findings indicate that the earlier recommendations regarding the performance of these functionals in σ^{2PA}

analyses could be linked to their consistent and reliable calculations of μ_{01}.[35,52] Furthermore, our recent research has revealed that μ_{01} is a critical factor in determining σ^{2PA} values of coumarin dyes in various solvents.[3] Interestingly, a specific assessment of the performance of LDA (S-VWN), GGA (PBE), and H-GGA (B3LYP, BHandHLYP, PBE0) functionals on the basis of their MAEs in μ_{01} suggests a potential ranking based on their respective % HF E_x. In contrast, the analysis of other functionals reveals that the contributions from the SR and LR components do not affect their efficacy. An interesting performance stems from ωB97X, which despite its lower ranking in μ_{01} accuracy, emerges as the top functional in computing μ_{00}, closely succeeded by ωB97X-V.

In the context of μ_{00} calculations, none of the LDA, GGA, or H-GGA functionals are found within the top nine. Instead, this group is led by RSH-GGA and HM-GGA functionals (M11, M06, M06-2X). However, poorly performing exceptions like CAM-QTP-00 and LRC-ωPBEh are found with MAEs of 0.52 and 0.53 Debye, respectively. A similar overall trend is observed in the computation of μ_{11}, where RSH-GGA and HM-GGA (M11, M06, M06-2X) also predominate. Distinctively, M11, LC-QTP, and M06-2X exhibit the lowest MAEs of 1.81, 1.91, and 2.16 Debye, respectively. Thus, diverging from their respective performances in μ_{01} and μ_{00} evaluations. Moreover, analysis shows that the QTP variants prove to be reliable in predicting both μ_{00} and μ_{11}.

With respect to the evaluation of $\Delta\mu$, M11 emerges as the leading functional (MAE = 3.33 Debye), closely followed by LC-QTP and M06-2X. In contrast, ωB97X, despite excelling for μ_{00}, exhibits a larger MAE in $\Delta\mu$ computations (MAE = 3.71 Debye). While $\Delta\mu$ calculations involve inherent cancellation of errors, this parameter is crucial in the 2PA calculations due to its contribution to 2PA intensities.[36,37,115]

The results from our MAEs and μ magnitude computations suggest a preferred suite of functionals for various μ calculations. This includes M11, M06-2X, QTP variants (excluding CAM-QTP-00), ωB97X, ωB97X-V, and CAM-B3LYP, each showcasing commendable per-

formance across different values: μ_{00}, μ_{11}, $\Delta\mu$, and μ_{01}. Among these, M11, M06-2X, and the QTP variants are particularly recommended for their efficacy in computing values of μ.

4 Conclusions

This study explored and evaluated a wide range of DFT functionals for the excitation from S_0 to S_1, using response theory, encompassing LDA, GGA, H-GGA, RSH-GGA, M-GGA, and HM-GGA, in their ability to reliably calculate the 2PA cross-sections, σ^{2PA}, and associated dipole moments, μ_{00}, μ_{11}, $\Delta\mu$, μ_{01} for a series of coumarin dyes. The systematic analysis of these functionals, which was evaluated relative to RI-CC2 results, aids in understanding their efficacy in predicting these critical photophysical parameters.

Functionals that outperform others in predicting σ^{2PA} were identified as those integrating SR and LR electron correlation effects effectively, namely RSH and HM-GGA. The range-separation approach in these functionals is more influential than the hybrid approach. While HF E_x is impactful in hybrid methods, it is the interplay of SR and LR effects that proves most crucial. In this context, functionals like M11, various QTP variants, ωB97X (including ωB97X-V), and M06-2X have demonstrated superior performance over others, including the widely used CAM-B3LYP functional, suggesting the importance of a comprehensive parametrization approach.

In the computations of dipole moments, μ_{01}, μ_{00}, μ_{11}, and $\Delta\mu$, which are crucial for understanding σ^{2PA} computations within the 2SM, functionals like M11, M06-2X, QTP variants, and ωB97X (including ωB97X-V) consistently yielded reliable results. In μ_{01} computations, the influence of HF E_x was more pronounced than range-separation. However, this pattern was not observed in the calculations of μ_{00}, μ_{11}, and $\Delta\mu$, where the dominance of range-separation was clear, particularly in the performance of M11, M06-2X, and QTP variants. This indicates the robust capability of these functionals, with emphasis on M11 and M06-

2X, in modeling electronic transitions and electron density distributions across various dipole moments.

While the current study focused on specific coumarin dyes, the implications of our findings could extend to a wider range of fluorescent dyes. It is recommended that the functionals identified for their effectiveness in this research be applied in subsequent analyses of other fluorescent dyes. Such an approach would not only expand the scope of our understanding but also further validate their applicability in 2PA processes.

Acknowledgement

I.A.E acknowledges the support of the Natural Sciences and Engineering Research Council of Canada (NSERC) through a Postgraduate Scholarship–Doctoral (PGS D) award. R.A.M thanks the Brazilian agency CNPq (Grants:401125/2022-0 and 403961/2021-1) for funding support. A.B. thanks NSERC for a Discovery Grant. The authors thank the Digital Research Alliance of Canada for the computing resources.

Supporting Information Available

The Cartesian coordinates of the optimized geometries, excitation energies, dipole moments, 2PA cross-sections, 2PA transition strengths, and mean absolute errors are provided free of charge in the Supporting Information.

References

(1) Göppert-Mayer, M. Über Elementarakte Mit Zwei Quantensprüngen. *Ann. Phys. (Berl.)* **1931**, *401*, 273–294.

(2) Kaiser, W.; Garrett, C. Two-Photon Excitation in CaF_2:Eu^{2+}. *Phys. Rev. Lett.* **1961**, *7*, 229.

(3) Elayan, I. A.; Brown, A. Degenerate and Non-Degenerate Two-Photon Absorption of Coumarin Dyes. *Phys. Chem. Chem. Phys.* **2023**, *25*, 16772–16780.

(4) De Wergifosse, M.; Houk, A. L.; Krylov, A. I.; Elles, C. G. Two-Photon Absorption Spectroscopy of Trans-Stilbene, Cis-Stilbene, and Phenanthrene: Theory and Experiment. *J. Chem. Phys.* **2017**, *146*, 144305.

(5) Hales, J. M.; Hagan, D. J.; Van Stryland, E. W.; Schafer, K.; Morales, A.; Belfield, K. D.; Pacher, P.; Kwon, O.; Zojer, E.; Brédas, J.-L. Resonant Enhancement of Two-Photon Absorption in Substituted Fluorene Molecules. *J. Chem. Phys.* **2004**, *121*, 3152–3160.

(6) Drobizhev, M.; Makarov, N. S.; Rebane, A.; de la Torre, G.; Torres, T. Strong Two-Photon Absorption in Push- Pull Phthalocyanines: Role of Resonance Enhancement and Permanent Dipole Moment Change upon Excitation. *J. Phys. Chem. C* **2008**, *112*, 848–859.

(7) Pascal, S.; David, S.; Andraud, C.; Maury, O. Near-Infrared Dyes for Two-Photon Absorption in the Short-Wavelength Infrared: Strategies Towards Optical Power Limiting. *Chem. Soc. Rev.* **2021**, *50*, 6613–6658.

(8) Denk, W.; Strickler, J. H.; Webb, W. W. Two-Photon Laser Scanning Fluorescence Microscopy. *Science* **1990**, *248*, 73–76.

(9) Xu, C.; Zipfel, W.; Shear, J. B.; Williams, R. M.; Webb, W. W. Multiphoton Fluorescence Excitation: New Spectral Windows for Biological Nonlinear Microscopy. *Proc. Natl. Acad. Sci. U.S.A.* **1996**, *93*, 10763–10768.

(10) Ogawa, K.; Kobuke, Y. Design of Two-Photon Absorbing Materials for Molecular Optical Memory and Photodynamic Therapy. *Org. Biomol. Chem.* **2009**, *7*, 2241–2246.

(11) Celli, J. P.; Spring, B. Q.; Rizvi, I.; Evans, C. L.; Samkoe, K. S.; Verma, S.; Pogue, B. W.; Hasan, T. Imaging and Photodynamic Therapy: Mechanisms, Monitoring, and Optimization. *Chem. Rev.* **2010**, *110*, 2795–2838.

(12) Cumpston, B. H.; Ananthavel, S. P.; Barlow, S.; Dyer, D. L.; Ehrlich, J. E.; Erskine, L. L.; Heikal, A. A.; Kuebler, S. M.; Lee, I.-Y. S.; McCord-Maughon, D.; others Two-Photon Polymerization Initiators for Three-Dimensional Optical Data Storage and Microfabrication. *Nature* **1999**, *398*, 51–54.

(13) Belfield, K. D.; Schafer, K. J.; Liu, Y.; Liu, J.; Ren, X.; Stryland, E. W. V. Multiphoton-Absorbing Organic Materials for Microfabrication, Emerging Optical Applications, and Non-Destructive Three-Dimensional Imaging. *J. Phys. Org. Chem.* **2000**, *13*, 837–849.

(14) Strickler, J. H.; Webb, W. W. Three-Dimensional Optical Data Storage in Refractive Media by Two-Photon Point Excitation. *Opt. Lett.* **1991**, *16*, 1780–1782.

(15) Dvornikov, A.; Walker, E.; Rentzepis, P. Two-Photon Three-Dimensional Optical Storage Memory. *J. Phys. Chem. A* **2009**, *113*, 13633–13644.

(16) Pawlicki, M.; Collins, H. A.; Denning, R. G.; Anderson, H. L. Two-photon Absorption and the Design of Two-Photon Dyes. *Angew. Chem. Int. Ed.* **2009**, *48*, 3244–3266.

(17) Alam, M. M.; Chattopadhyaya, M.; Chakrabarti, S.; Ruud, K. High-Polarity Solvents Decreasing the Two-Photon Transition Probability of Through-Space Charge-Transfer Systems – A Surprising In Silico Observation. *J. Phys. Chem. Lett.* **2012**, *3*, 961–966.

(18) Wielgus, M.; Zaleśny, R.; Murugan, N. A.; Kongsted, J.; Ågren, H.; Samoc, M.; Bartkowiak, W. Two-Photon Solvatochromism II: Experimental and Theoretical Study of Solvent Effects on the Two-Photon Absorption Spectrum of Reichardt's Dye. *ChemPhysChem* **2013**, *14*, 3731–3739.

(19) Beerepoot, M. T.; Friese, D. H.; Ruud, K. Intermolecular Charge Transfer Enhances Two-Photon Absorption in Yellow Fluorescent Protein. *Phys. Chem. Chem. Phys.* **2014**, *16*, 5958–5964.

(20) He, G. S.; Tan, L.-S.; Zheng, Q.; Prasad, P. N. Multiphoton Absorbing Materials: Molecular Designs, Characterizations, and Applications. *Chem. Rev.* **2008**, *108*, 1245–1330.

(21) Drobizhev, M.; Makarov, N. S.; Tillo, S. E.; Hughes, T. E.; Rebane, A. Two-Photon Absorption Properties of Fluorescent Proteins. *Nat. Methods* **2011**, *8*, 393–399.

(22) Zilbershtein-Shklanovsky, L.; Weitman, M.; Major, D. T.; Fischer, B. Rules for The Design of Highly Fluorescent Nucleoside Probes: 8-(Substituted Cinnamyl)-Adenosine Analogues. *J. Org. Chem.* **2013**, *78*, 11999–12008.

(23) Dudley, C. Chromophore Design for Large Two-Photon Absorption. *Opt. Mater.* **2014**, *37*, 750–755.

(24) Gedik, M.; Brown, A. Computational Study of The Excited State Properties of Modified RNA Nucleobases. *J. Photochem. Photobiol. A* **2013**, *259*, 25–32.

(25) Liu, H.; Ge, C.; Yu, G.; Qian, X. Theoretical Study of The Structural and Optical Properties of Cytosine Analogues. *Comput. Theor. Chem.* **2014**, *1049*, 75–81.

(26) De Wergifosse, M.; Beaujean, P.; Grimme, S. Ultrafast Evaluation of Two-Photon Ab-

sorption with Simplified Time-Dependent Density Functional Theory. *J. Phys. Chem. A* **2022**, *126*, 7534–7547.

(27) Zhao, Y.; Cui, X.; Ge, Z.; Meng, Q.; Zhang, C. Unusual Photophysical Properties of Fluorescent Cytosine Analogues Utilized in Real-Time Detecting i-Motif DNA: A Theoretical Study. *J. Lumin.* **2021**, *240*, 118442.

(28) Zhao, Y.; Cui, X.; Song, Y.; Zhang, C.; Meng, Q. Photophysical Properties of Fluorescent Nucleobase P-Analogues Expected to Monitor DNA Replication. *Spectrochim. Acta A Mol. Biomol. Spectrosc.* **2021**, *260*, 119926.

(29) Jacquemin, D.; Perpète, E. A.; Scalmani, G.; Frisch, M. J.; Assfeld, X.; Ciofini, I.; Adamo, C. Time-Dependent Density Functional Theory Investigation of the Absorption, Fluorescence, and Phosphorescence Spectra of Solvated Coumarins. *J. Chem. Phys.* **2006**, *125*, 164324.

(30) Adamo, C.; Jacquemin, D. The Calculations of Excited-State Properties with Time-Dependent Density Functional Theory. *Chem Soc Rev* **2013**, *42*, 845–856.

(31) Loos, P.-F.; Comin, M.; Blase, X.; Jacquemin, D. Reference Energies for Intramolecular Charge-Transfer Excitations. *J. Chem. Theory Comput.* **2021**, *17*, 3666–3686.

(32) Chrayteh, A.; Blondel, A.; Loos, P.-F.; Jacquemin, D. Mountaineering Strategy to Excited States: Highly Accurate Oscillator Strengths and Dipole Moments of Small Molecules. *J. Chem. Theory Comput.* **2020**, *17*, 416–438.

(33) Sarkar, R.; Boggio-Pasqua, M.; Loos, P.-F.; Jacquemin, D. Benchmarking TD-DFT and Wave Function Methods for Oscillator Strengths and Excited-State Dipole Moments. *J. Chem. Theory Comput.* **2021**, *17*, 1117–1132.

(34) Hait, D.; Head-Gordon, M. How Accurate Is Density Functional Theory at Predicting Dipole Moments? An Assessment Using a New Database of 200 Benchmark Values. *J. Chem. Theory Comput.* **2018**, *14*, 1969–1981.

(35) Sirimatayanant, S.; Andruniów, T. Benchmarking Two-Photon Absorption Strengths of Rhodopsin Chromophore Models with CC3 and CCSD Methodologies: An Assessment of Popular Density Functional Approximations. *J. Chem. Phys.* **2023**, *158*, 094106.

(36) Beerepoot, M. T.; Friese, D. H.; List, N. H.; Kongsted, J.; Ruud, K. Benchmarking Two-Photon Absorption Cross Sections: Performance of CC2 and CAM-B3LYP. *Phys. Chem. Chem. Phys.* **2015**, *17*, 19306–19314.

(37) Rossano-Tapia, M.; Brown, A. Quantum Mechanical/Molecular Mechanical Studies of Photophysical Properties of Fluorescent Proteins. *Wiley Interdiscip. Rev. Comput. Mol. Sci.* **2022**, *12*, e1557.

(38) Christiansen, O.; Koch, H.; Jørgensen, P. The Second-Order Approximate Coupled Cluster Singles and Doubles Model CC2. *Chem. Phys. Lett.* **1995**, *243*, 409–418.

(39) Friese, D. H.; Hättig, C.; Ruud, K. Calculation of Two-Photon Absorption Strengths with the Approximate Coupled Cluster Singles and Doubles Model CC2 Using the Resolution-of-Identity Approximation. *Phys. Chem. Chem. Phys.* **2012**, *14*, 1175–1184.

(40) Runge, E.; Gross, E. K. Density-Functional Theory for Time-Dependent Systems. *Phys. Rev. Lett.* **1984**, *52*, 997.

(41) Beerepoot, M. T.; Alam, M. M.; Bednarska, J.; Bartkowiak, W.; Ruud, K.; Zaleśny, R. Benchmarking the Performance of Exchange-Correlation Functionals for Predicting Two-Photon Absorption Strengths. *J. Chem. Theory Comput.* **2018**, *14*, 3677–3685.

(42) Chołuj, M.; Alam, M. M.; Beerepoot, M. T.; Sitkiewicz, S. P.; Matito, E.; Ruud, K.; Zaleśny, R. Choosing Bad versus Worse: Predictions of Two-Photon-Absorption Strengths Based on Popular Density Functional Approximations. *J. Chem. Theory Comput.* **2022**, *18*, 1046–1060.

(43) Cave, R. J.; Castner, E. W. Time-Dependent Density Functional Theory Investigation of the Ground and Excited States of Coumarins 102, 152, 153, and 343. *J. Phys. Chem. A* **2002**, *106*, 12117–12123.

(44) Preat, J.; Jacquemin, D.; Wathelet, V.; André, J.-M.; Perpète, E. A. TD-DFT Investigation of the UV Spectra of Pyranone Derivatives. *J. Phys. Chem. A* **2006**, *110*, 8144–8150.

(45) Jacquemin, D.; Perpète, E. A.; Assfeld, X.; Scalmani, G.; Frisch, M. J.; Adamo, C. The Geometries, Absorption and Fluorescence Wavelengths of Solvated Fluorescent Coumarins: A CIS and TD-DFT Comparative Study. *Chem. Phys. Lett.* **2007**, *438*, 208–212.

(46) List, N. H.; Olsen, J. M.; Rocha-Rinza, T.; Christiansen, O.; Kongsted, J. Performance of Popular XC-Functionals for the Description of Excitation Energies in GFP-Like Chromophore Models. *Int. J. Quantum Chem.* **2012**, *112*, 789–800.

(47) Grabarz, A. M.; Ośmiałowski, B. Benchmarking Density Functional Approximations for Excited-State Properties of Fluorescent Dyes. *Molecules* **2021**, *26*, 7434.

(48) Helal, W. Double Hybrid Density Functionals for the Electronic Excitation Energies of Linear Cyanines. *J. Phys. Chem. A* **2022**, *127*, 131–141.

(49) Alkhatib, Q.; Helal, W.; Marashdeh, A. Accurate Predictions of the Electronic Excited States of BODIPY-Based Dye Sensitizers Using Spin-Component-Scaled Double-Hybrid Functionals: A TD-DFT Benchmark Study. *RSC Adv.* **2022**, *12*, 1704–1717.

(50) Salem, M. A.; Brown, A. Two-Photon Absorption in Fluorescent Protein Chromophores: TDDFT and CC2 results. *J. Chem. Theory Comput.* **2014**, *10*, 3260–3269.

(51) Rossano-Tapia, M.; Brown, A. Determination of Two-Photon-Absorption Cross Sections Using Time-Dependent Density Functional Theory Tight Binding: Application to Fluorescent Protein Chromophores. *J. Chem. Theory Comput.* **2019**, *15*, 3153–3161.

(52) Grabarek, D.; Andruniów, T. Assessment of Functionals for TDDFT Calculations of One-and Two-Photon Absorption Properties of Neutral and Anionic Fluorescent Proteins Chromophores. *J. Chem. Theory Comput.* **2018**, *15*, 490–508.

(53) Grabarek, D.; Andruniów, T. Illuminating the Origins of Two-Photon Absorption Properties in Fluorescent Protein Chromophores. *Int. J. Quantum Chem.* **2020**, *120*, e26086.

(54) Salem, M. A.; Brown, A. Two-Photon Absorption of Fluorescent Protein Chromophores Incorporating Non-Canonical Amino Acids: TD-DFT Screening and Classical Dynamics. *Phys. Chem. Chem. Phys.* **2015**, *17*, 25563–25571.

(55) TURBOMOLE V7.3 2018, A Development of University of Karlsruhe and Forschungszentrum Karlsruhe GmbH, 1989-2007, TURBOMOLE GmbH, since 2007; available from http://www.turbomole.com.

(56) Furche, F.; Ahlrichs, R.; Hättig, C.; Klopper, W.; Sierka, M.; Weigend, F. Turbomole. *Wiley Interdiscip. Rev. Comput. Mol. Sci.* **2014**, *4*, 91–100.

(57) Zhang, W.; Huo, F.; Cheng, F.; Yin, C. Employing an ICT-FRET Integration Platform for the Real-Time Tracking of SO_2 Metabolism in Cancer Cells and Tumor Models. *J. Am. Chem. Soc.* **2020**, *142*, 6324–6331.

(58) Niu, H.; Zhang, Y.; Zhao, F.; Mo, S.; Cao, W.; Ye, Y.; Zhao, Y. Reductive Stress Imaging in the Endoplasmic Reticulum by Using Living Cells and Zebrafish. *Chem. Commun.* **2019**, *55*, 9629–9632.

(59) Kong, X.; Li, M.; Dong, B.; Zhang, N.; Song, W.; Lu, Y.; Lin, W. A Near-Infrared and Two-Photon Dual-Mode Fluorescent Probe for the Colorimetric Monitoring of SO_2 in Vitro and in Vivo. *Analyst* **2019**, *144*, 4371–4379.

(60) Xu, H.; Zhang, H.; Liu, G.; Kong, L.; Zhu, X.; Tian, X.; Zhang, Z.; Zhang, R.; Wu, Z.; Tian, Y.; others Coumarin-Based Fluorescent Probes for Super-Resolution and Dynamic Tracking of Lipid Droplets. *Anal. Chem.* **2018**, *91*, 977–982.

(61) Agrawal, A.; Siddiqui, S. A.; Soni, A.; Sharma, G. D. Advancements, Frontiers and Analysis of Metal Oxide Semiconductor, Dye, Electrolyte and Counter Electrode of Dye Sensitized Solar Cell. *Sol. Energy.* **2022**, *233*, 378–407.

(62) Chalil Oglou, R.; Ulusoy Ghobadi, T. G.; Ozbay, E.; Karadas, F. "Plug and Play" Photosensitizer–Catalyst Dyads for Water Oxidation. *ACS Appl. Mater. Interfaces.* **2022**, *14*, 21131–21140.

(63) Christie, R. M.; Lui, C.-H. Studies of Fluorescent Dyes: Part 2. An Investigation of the Synthesis and Electronic Spectral Properties of Substituted 3-(2′-Benzimidazolyl) Coumarins. *Dyes Pigm.* **2000**, *47*, 79–89.

(64) Nanda, K. D.; Krylov, A. I. Two-Photon Absorption Cross Sections Within Equation-of-Motion Coupled-Cluster Formalism Using Resolution-of-the-Identity and Cholesky Decomposition Representations: Theory, Implementation, and Benchmarks. *J. Chem. Phys.* **2015**, *142*, 064118.

(65) Schmidt, M. W.; Baldridge, K. K.; Boatz, J. A.; Elbert, S. T.; Gordon, M. S.;

Jensen, J. H.; Koseki, S.; Matsunaga, N.; Nguyen, K. A.; Su, S.; others General Atomic and Molecular Electronic Structure System. *J. Comput. Chem.* **1993**, *14*, 1347–1363.

(66) Aidas, K.; Angeli, C.; Bak, K. L.; Bakken, V.; Bast, R.; Boman, L.; Christiansen, O.; Cimiraglia, R.; Coriani, S.; Dahle, P.; others The Dalton Quantum Chemistry Program System. *Wiley Interdiscip. Rev. Comput. Mol. Sci.* **2014**, *4*, 269–284.

(67) Jacquemin, D.; Planchat, A.; Adamo, C.; Mennucci, B. TD-DFT Assessment of Dunctionals for Optical 0–0 Transitions in Solvated Dyes. *J. Chem. Theory Comput.* **2012**, *8*, 2359–2372.

(68) Grabarek, D.; Andruniów, T. The Role of Hydrogen Bonds and Electrostatic Interactions in Enhancing Two-Photon Absorption in Green and Yellow Fluorescent Proteins. *ChemPhysChem* **2022**, *23*, e202200003.

(69) Schwabe, T.; Beerepoot, M. T.; Olsen, J. M. H.; Kongsted, J. Analysis of Computational Models for an Accurate Study of Electronic Excitations in GFP. *Phys. Chem. Chem. Phys.* **2015**, *17*, 2582–2588.

(70) Shao, Y.; Gan, Z.; Epifanovsky, E.; Gilbert, A. T.; Wormit, M.; Kussmann, J.; Lange, A. W.; Behn, A.; Deng, J.; Feng, X.; others Advances in Molecular Quantum Chemistry Contained in the Q-Chem 4 Program Package. *Mol. Phys.* **2015**, *113*, 184–215.

(71) Niehaus, T. A.; Della Sala, F. Range Separated Functionals in the Density Functional Based Tight-Binding Method: Formalism. *Phys. Status Solidi B* **2012**, *249*, 237–244.

(72) Rinkevicius, Z.; Li, X.; Vahtras, O.; Ahmadzadeh, K.; Brand, M.; Ringholm, M.; List, N. H.; Scheurer, M.; Scott, M.; Dreuw, A.; others VeloxChem: A Python-Driven Density-Functional Theory Program for Spectroscopy Simulations in High-

Performance Computing Environments. *Wiley Interdiscip. Rev. Comput. Mol. Sci.* **2020**, *10*, e1457.

(73) Ahmadzadeh, K.; Li, X.; Rinkevicius, Z.; Norman, P.; Zaleśny, R. Toward Accurate Two-Photon Absorption Spectrum Simulations: Exploring the Landscape beyond the Generalized Gradient Approximation. *J. Phys. Chem. Lett.* **2024**, *15*, 969–974.

(74) Verma, P.; Bartlett, R. J. Increasing the Applicability of Density Functional Theory. IV. Consequences of Ionization-Potential Improved Exchange-Correlation Potentials. *J. Chem. Phys.* **2014**, *140*, 18A534.

(75) Jin, Y.; Bartlett, R. J. The QTP Family of Consistent Functionals and Potentials in Kohn-Sham Density Functional Theory. *J. Chem. Phys.* **2016**, *145*, 034107.

(76) Haiduke, R. L. A.; Bartlett, R. J. Non-Empirical Exchange-Correlation Parameterizations Based on Exact Conditions from Correlated Orbital Theory. *J. Chem. Phys.* **2018**, *148*, 184106.

(77) Bartlett, R. J. Towards an Exact Correlated Orbital Theory for Electrons. *Chem. Phys. Lett.* **2009**, *484*, 1–9.

(78) Mendes, R. A.; Haiduke, R. L.; Bartlett, R. J. The Devil's Triangle of Kohn–Sham Density Functional Theory and Excited States. *J. Chem. Phys.* **2021**, *154*, 074106.

(79) Frisch, M.; Trucks, G.; Schlegel, H.; Scuseria, G.; Robb, M.; Cheeseman, J.; Scalmani, G.; Barone, V.; Petersson, G.; Nakatsuji, H.; others Gaussian 16. 2016.

(80) Lee, C.; Yang, W.; Parr, R. G. Development of the Colle-Salvetti Correlation-Energy Formula into a Functional of the Electron Density. *Phys. Rev. B* **1988**, *37*, 785.

(81) Becke, A. D. Density-Functional Thermochemistry. I. The Effect of the Exchange-Only Gradient Correction. *J. Chem. Phys.* **1992**, *96*, 2155–2160.

(82) Grimme, S.; Antony, J.; Ehrlich, S.; Krieg, H. A Consistent and Accurate Ab Initio Parametrization of Density Functional Dispersion Correction (DFT-D) for the 94 Elements H-Pu. *J. Chem. Phys.* **2010**, *132*, 154104.

(83) Grimme, S.; Ehrlich, S.; Goerigk, L. Effect of the Damping Function in Dispersion Corrected Density Functional Theory. *J. Comput. Chem.* **2011**, *32*, 1456–1465.

(84) Becke, A. D.; Johnson, E. R. A Density-Functional Model of the Dispersion Interaction. *J. Chem. Phys.* **2005**, *123*, 154101.

(85) Johnson, E. R.; Becke, A. D. A Post-Hartree-Fock Model of Intermolecular Interactions: Inclusion of Higher-Order Corrections. *J. Chem. Phys.* **2006**, *124*, 174104.

(86) Casida, M. E. *Recent Advances In Density Functional Methods: (Part I)*; World Scientific, 1995; pp 155–192.

(87) Dunning Jr, T. H. Gaussian Basis Sets for Use in Correlated Molecular Calculations. I. The Atoms Boron through Neon and Hydrogen. *J. Chem. Phys.* **1989**, *90*, 1007–1023.

(88) Woon, D. E.; Dunning Jr, T. H. Gaussian Basis Sets for Use in Correlated Molecular Calculations. V. Core-Valence Basis Sets for Boron through Neon. *J. Chem. Phys.* **1995**, *103*, 4572–4585.

(89) Koch, H.; Jørgensen, P. Coupled Cluster Response Functions. *J. Chem. Phys.* **1990**, *93*, 3333.

(90) Hättig, C.; Weigend, F. CC2 Excitation Energy Calculations on Large Molecules Using the Resolution of the Identity Approximation. *J. Chem. Phys.* **2000**, *113*, 5154–5161.

(91) Slater, J. C.; Johnson, K. H. Self-Consistent-Field $X\alpha$ Cluster Method for Polyatomic Molecules and Solids. *Phys. Rev. B* **1972**, *5*, 844.

(92) Vosko, S. H.; Wilk, L.; Nusair, M. Accurate Spin-Dependent Electron Liquid Correlation Energies for Local Spin Density Calculations: A Critical Analysis. *Can. J. Phys.* **1980**, *58*, 1200–1211.

(93) Perdew, J. P.; Burke, K.; Ernzerhof, M. Generalized Gradient Approximation Made Simple. *Phys. Rev. Lett.* **1996**, *77*, 3865.

(94) Becke, A. D. Density-Functional Exchange-Energy Approximation with Correct Asymptotic Behavior. *Phys. Rev. A* **1988**, *38*, 3098.

(95) Lee, C.; Yang, W.; Parr, R. G. Development of the Colle-Salvetti Correlation-Energy Formula into a Functional of the Electron Density. *Phys. Rev. B* **1988**, *37*, 785.

(96) Becke, A. D. A New Mixing of Hartree–Fock and Local Density-Functional Theories. *J. Chem. Phys.* **1993**, *98*, 1372–1377.

(97) Stephens, P. J.; Devlin, F. J.; Chabalowski, C. F.; Frisch, M. J. Ab Initio Calculation of Vibrational Absorption and Circular Dichroism Spectra Using Density Functional Force Fields. *J. Phys. Chem.* **1994**, *98*, 11623–11627.

(98) Adamo, C.; Barone, V. Toward Reliable Density Functional Methods without Adjustable Parameters: The PBE0 Model. *J. Chem. Phys.* **1999**, *110*, 6158–6170.

(99) Yanai, T.; Tew, D. P.; Handy, N. C. A New Hybrid Exchange–Correlation Functional Using the Coulomb-Attenuating Method (CAM-B3LYP). *Chem. Phys. Lett.* **2004**, *393*, 51–57.

(100) Chai, J.-D.; Head-Gordon, M. Systematic Optimization of Long-Range Corrected Hybrid Density Functionals. *J. Chem. Phys.* **2008**, *128*, 084106.

(101) Mardirossian, N.; Head-Gordon, M. ωB97X-V: A 10-Parameter, Range-Separated Hybrid, Generalized Gradient Approximation Density Functional with Nonlocal Correla-

tion, Designed by a Survival-of-the-Fittest Strategy. *Phys. Chem. Chem. Phys.* **2014**, *16*, 9904–9924.

(102) Rohrdanz, M. A.; Martins, K. M.; Herbert, J. M. A Long-Range-Corrected Density Functional That Performs Well for Both Ground-State Properties and Time-Dependent Density Functional Theory Excitation Energies, Including Charge-Transfer Excited States. *J. Chem. Phys.* **2009**, *130*, 054112.

(103) Tao, J.; Perdew, J. P.; Staroverov, V. N.; Scuseria, G. E. Climbing the Density Functional Ladder: Nonempirical Meta-Generalized Gradient Approximation Designed for Molecules and Solids. *Phys. Rev. Lett.* **2003**, *91*, 146401.

(104) Peverati, R.; Truhlar, D. G. Improving the Accuracy of Hybrid Meta-GGA Density Functionals by Range Separation. *J. Phys. Chem. Lett.* **2011**, *2*, 2810–2817.

(105) Zhao, Y.; Truhlar, D. G. The M06 Suite of Density Functionals for Main Group Thermochemistry, Thermochemical Kinetics, Noncovalent Interactions, Excited States, and Transition Elements: Two New Functionals and Systematic Testing of Four M06-Class Functionals and 12 Other Functionals. *Theor. Chem. Acc.* **2008**, *120*, 215–241.

(106) Zhao, Y.; Truhlar, D. G. A New Local Density Functional for Main-Group Thermochemistry, Transition Metal Bonding, Thermochemical Kinetics, and Noncovalent Interactions. *J. Chem. Phys.* **2006**, *125*, 194101.

(107) Staroverov, V. N.; Scuseria, G. E.; Tao, J.; Perdew, J. P. Comparative Assessment of a New Nonempirical Density Functional: Molecules and Hydrogen-Bonded Complexes. *J. Chem. Phys.* **2003**, *119*, 12129–12137.

(108) Laurent, A. D.; Jacquemin, D. TD-DFT Benchmarks: A Review. *Int. J. Quantum Chem.* **2013**, *113*, 2019–2039.

(109) Kaila, V. R.; Send, R.; Sundholm, D. Electrostatic Spectral Tuning Mechanism of the Green Fluorescent Protein. *Phys. Chem. Chem. Phys.* **2013**, *15*, 4491–4495.

(110) Grotjahn, R.; Furche, F. Gauge-Invariant Excited-State Linear and Quadratic Response Properties within the Meta-Generalized Gradient Approximation. *J. Chem. Theory Comput.* **2023**, *19*, 4897–4911.

(111) Zhao, Y.; Truhlar, D. G. The M06 Suite of Density Functionals for Main Group Thermochemistry, Thermochemical Kinetics, Noncovalent Interactions, Excited States, and Transition Elements: Two New Functionals and Systematic Testing of Four M06-Class Functionals and 12 Other Functionals. *Theor. Chem. Acc.* **2008**, *120*, 215–241.

(112) Zhao, Y.; Truhlar, D. G. Applications and Validations of the Minnesota Density Functionals. *Chem. Phys. Lett.* **2011**, *502*, 1–13.

(113) Alipour, M. Theoretical Prediction of Valence and Rydberg Excited States: Minnesota Exchange-Correlation Functionals vs. Symmetry-Adapted Cluster-Configuration Interaction. *Int. J. Quantum Chem.* **2019**, *119*, e25898.

(114) Steinbuch, K. B.; Tor, Y. *Handbook of Chemical Biology of Nucleic Acids*; Springer, 2023; pp 1–24.

(115) Salem, M. A.; Twelves, I.; Brown, A. Prediction of Two-Photon Absorption Enhancement in Red Fluorescent Protein Chromophores Made from Non-Canonical Amino Acids. *Phys. Chem. Chem. Phys.* **2016**, *18*, 24408–24416.